1 ***Revision 2***

2 Word Count: 7638

3 **Continuous Be mineralization from two-mica granite to pegmatite:**
4 **Critical element enrichment processes in a Himalayan leucogranite**
5 **pluton**

6

7 CHEN LIU[1, 2], RU-CHENG WANG[1, 2]*, ROBERT L. LINNEN[3], FU-YUAN WU[4], LEI
8 XIE[1, 2], XIAO-CHI LIU[4]

9

10 [1]*State Key Laboratory for Mineral Deposits Research, School of Earth Sciences and Engineering,*
11 *Nanjing University, Nanjing 210023, China*

12 [2]*Frontiers Science Center for Critical Earth Material Cycling, Nanjing University, Nanjing*
13 *210023, China*

14 [3]*Department of Earth Sciences, Western University, 1151 Richmond St, London, Ontario N6A 3K7,*
15 *Canada*

16 [4]*State Key Laboratory of Lithospheric Evolution, and Institutions of Earth Science, Institute of*
17 *Geology and Geophysics, Chinese Academy of Sciences, Beijing 100029, China*

18

19 **Corresponding author: Rucheng Wang (rcwang@nju.edu.cn)*

20

ABSTRACT

Beryllium is a critical metal typically concentrated in highly fractionated granitic rocks such as the leucogranites in the Himalaya. Here, we report beryl mineralization continuous from the earlier and less evolved two-mica granite to the highly evolved albite granite and pegmatite in a typical leucogranite pluton at Pusila in the central of Himalaya. Textural and mineral chemical evidences support a magmatic origin for beryl, and the trends of beryl crystal chemistry indicate magma differentiation. Despite low to moderate fractionation of the biotite granite and two-mica granite in the Pusila leucogranite pluton, the Be contents (~7 μg/g, beryl-free and ~22 μg/g, beryl-bearing, respectively) of these granites are much higher than the average for biotite- and two-mica granites worldwide (~3–4, and 5–10 μg/g, respectively), indicating that the initial magma had a relatively high Be concentration. The gneisses of Greater Himalayan System, considered as the protolith, also show a higher Be abundance (~4–6 μg/g) than the mean value of pelitic rocks worldwide (~2–3 μg/g), which could be the source reservoir of Be. The source contributed the initial Be to the melt and fractionation resulted in the onset of beryl crystallization from the interstitial residual melt in the two-mica granite. The ubiquity of beryl in two-mica granite to pegmatite stages of the Pusila pluton is explained by a continuous crystallization model, although there was a delay in the onset of beryl crystallization in the two-mica granite. Modeling based on Rayleigh fractionation indicates that Be becomes compatible once saturation is attained owing to the beryl crystallization. Our findings indicate that the enrichment of critical elements (e.g., Be) is controlled not only by

fractional crystallization, but also by the buffering action of a saturating phase (e.g., beryl) on the concentration of the critical element in the melt.

Keywords: Himalayan leucogranite, beryllium, beryl, source, fractionation, delayed crystallization

INTRODUCTION

Beryllium is a lithophile element that is considered as a critical metal, owing to its high demand in technologically strategic materials in next-generation industries (e.g., new energies, new alloys) (Chakhmouradian et al. 2014; Trueman and Sabey 2014; Sovacool et al. 2020). The world's largest beryllium deposit is the Spor Mountain in USA, a rhyolite-hosted deposit where the ore mineral is bertrandite. The remainder of global Be production is almost entirely from beryl, which is typically hosted by granitic pegmatites (Linnen et al. 2012), although phenakite may also be important at some deposits.

On average, granites contain only ~4–8 μg/g Be (Beus 1966; Norton and Redden 1990; London and Evensen 2002). Beryl saturation in granitic melts requires extreme fractionation and low temperatures (London 2008, 2015), consequently, Be mineralization is generally linked to highly-evolved granites, in particular to granitic pegmatites.

The Himalayan leucogranite belts are endowed in extensive beryl mineralization (Wang et al. 2017). Particularly, the Pusila pluton, west of Mount Everest, is an excellent site to study Be-Nb-Ta-Li mineralization (Liu et al. 2020). Beryl at this

location is widely present as a magmatic phase not only in highly evolved intrusions (albite granite and pegmatite), but unexpectedly also in the earlier, less evolved two-mica granite stage of the magmatic evolution. This striking first-order observation provides the opportunity to investigate the mechanisms involved in beryl mineralization, beginning with two-mica granite and continuing to pegmatite in the leucogranite pluton, which may be more complicated than simple fractionation in a granitic system.

In this study, we present the whole-rock chemical composition of beryl-bearing leucogranites in Pusila, together with the petrography and mineral chemistry of beryl, and characterize the initial Be mineralization in two-mica granite. The evolutionary mechanism(s) for continuous Be mineralization from moderately to highly evolved granites and pegmatites are then evaluated, which may offer new insights into the Be mineralization generally. Our results reveal that beryllium concentration is controlled concurrently by more than one process in melts, for example, fractional crystallization and the buffering action of beryl when the melt is saturated with beryl. This interpretation of the control on Be concentration might be applicable to other rare and incompatible elements.

GEOLOGICAL SETTING

Following the India–Asia continental collision beginning at ca. 55 Ma (Zhu et al. 2015), two sub-parallel, EW-trending belts of Cenozoic leucogranites intruded during the Himalayan orogeny. The northern belt was emplaced into the Tethyan Himalayan

sedimentary sequence, and the southern belt was emplaced within the Greater Himalayan crystalline sequence (GHS) (Le Fort et al. 1987). The Pusila leucogranite pluton crops out in the Rongxia Valley northwest of Mount Cho Oyu in the Mount Everest region, and was emplaced into the GHS (Fig. 1a).

The Pusila pluton crops out over an area of ~100 km^2, and is mainly composed of biotite granite, two-mica granite, muscovite granite, albite granite, and pegmatite, which progressively crop out with increasing altitude (from 3800 to 5400 m) (Figs. 1b–1c). This progression of granites crops out progressively along the Rongxia valley from south-west to north-east, with gradational contacts between the lithologies (Liu et al. 2020). Pegmatite typically forms dikes 0.5–3 meters thick and 10 to over 100 meters in extent cutting the country rocks near the upper parts of the Pusila pluton (Fig. 2). These pegmatites belong largely to the spodumene subtype (Černý and Ercit 2005) and are characterized by two stages of Li mineralization: a magmatic stage with primary spodumene and a hydrothermal stage with secondary spodumene and petalite (Liu et al. 2020).

SAMPLING AND ANALYTICAL METHODS

Samples

Sampling of the Pusila leucogranite pluton was carried out in the Rongxia Valley. The leucogranites of the Pusila pluton have gradational lithological changes, and we sampled typical biotite granite (3 samples) at an altitude of ~3800–3860 m, two-mica granite (10 samples) at ~3870–4600 m, muscovite granite (3 samples) at ~4600–5100

m, albite granite (5 samples) at ~5100–5340 m, and spodumene (-petalite) pegmatite (6 samples) at ~5200–5400 m (Figs. 1b–1c).

Whole-rock geochemistry

Whole-rock major element compositions were determined by wet chemical methods at the Analysis Center of the No. 230 Research Institute of the China National Nuclear Corporation (CNNC), Changsha, China. The procedures are described in the Chinese National standard protocol GB/T 14506-2010DZG93-05, and all errors on the reported concentrations are <5%. The trace element concentrations, including rare earth elements (REEs), were measured using an Agilent 7700X inductively coupled plasma mass spectrometry (ICP–MS) at Nanjing FocuMS Technology, Nanjing, China. Powdered samples (100 mg) were digested in 1 mL of concentrated HF and 0.5 mL of concentrated HNO_3 in PTFE-lined stainless-steel bombs at 190 °C for 72 h. Insoluble residues were dissolved by heating at 110 °C in 8 mL of 40 vol.% HNO_3 for 3 h (Qi et al. 2000). Standard reference materials (BHVO-2, AGV-2, W-2 and GSP-2 from the USGS) were used for calibration. Analytical precision for the REEs and other incompatible elements was better than ±10%. The detection limits (D.L.) of all analyzed elements are shown in Supplemental Data 1.

Imaging and major- and minor-element analyses of minerals

Analyses were conducted at the State Key Laboratory for Mineral Deposits Research in Nanjing University (MiDeR-NJU), China. Detailed pulse-colored mineral maps were produced with a Zeiss Sigma 300 field emission scanning electron microscope (FE-SEM) with a Bruker Quantax for energy-dispersive X-ray

spectroscopy (EDS). Back-scattered electron (BSE) images were obtained on polished thin-sections using a Zeiss Supra 55 field emission scanning electron microscope (FE-SEM) and a JEOL JXA-8230 electron microprobe.

The major and minor element concentrations of mineral phases were obtained using a JEOL JXA-8230 electron microprobe. The analyses (EMPA) were performed with an accelerating voltage of 15 kV, a probe current of 20 nA for all elements, and a beam diameter of 5 μm for micas, 3 μm for feldspars, and 1 μm for other minerals. Natural minerals (albite, fayalite, orthoclase, apatite, topaz, and hornblende) were used as standards for silicate mineral analysis, whereas natural minerals (fayalite and scheelite), synthetic metals (Nb, Ta, and Sc), and synthetic compounds (SnO_2 and $MnTiO_3$) were used as standards for oxide mineral analysis. The peak and background counting times for the major elements in each mineral were 10 and 5 s, respectively, and 20 and 10 s for other minor elements. All data were corrected using standard ZAF correction procedures, and the detection limits (D.L.) of all analyzed elements in minerals are shown in Supplemental Data 2.

In situ trace element analyses of minerals

In situ trace element analyses of beryl, micas, feldspars, tourmaline, and quartz were conducted by laser ablation (LA)–ICP–MS at MiDeR-NJU, China. A Photon Machines Excite LA system (RESOlution S-155) was used with a Thermo Fisher Scientific i-CAP-Q ICP–MS instrument. An ablation spot diameter of 43 μm was used for micas, feldspars, and tourmaline, with a repetition rate of 4 Hz and laser energy of 5.12 J/cm^2. An ablation spot diameter of 30 μm was used for beryl and quartz, with a

repetition rate of 4 Hz and laser energy of 5.36 J/cm^2. Helium was used as the carrier gas. National Institute of Standards and Technology (NIST) standard reference materials NIST-610 and NIST-612, and US Geological Survey basaltic glasses BCR-2G and GSE-1G were used as external standards, with ^{29}Si used as an internal standard to correct for instrument drift. Off-line data processing was performed using the ICPMSDataCal program (Liu et al. 2008). The estimated precision was better than ±5% for major elements and ± 10% for trace elements, and the detection limits (D.L.) of all analyzed elements in minerals are shown in Supplemental Data 2.

RESULTS

Whole-rock geochemistry

Whole-rock geochemical analyses show that all the granitoids are peraluminous, and display trends of increasing Na_2O content and decreasing CaO and Sr concentrations (Supplemental Data 1.1). From the biotite granite through two-mica granite and muscovite granite then to albite granite and pegmatite, some whole-rock compositional parameters show obvious trends, including the decrease in TiO_2 and REE contents, the increase in Rb/Sr and decrease in Zr/Hf and Nb/Ta ratios (Fig. 3; Supplemental Fig. S1). Empirical equations are used to calculate zircon (T_{Zr}) and monazite (T_{REE}) saturation temperatures (Watson and Harrison 1983; Montel 1993), which progressively decrease from ~780 °C (biotite granite) to ~550 °C (pegmatite) (Fig. 3c). These temperatures are within a realistic range for crystallization of Himalayan leucogranites (Scaillet et al. 1990; Ayres et al. 1997). However, the

pegmatite has a much lower T_{REE} than T_{Zr}. The large difference can be attributed either to the very low REE concentrations, which are at the limit of detection in pegmatite, or to the high Hf content of the zircons from pegmatite, a factor not considered in the calculation of T_{Zr}.

Rock-forming minerals

Rock-forming minerals contain trace amounts of Be (Table 1; Supplemental Data 2.2–2.5). The K-feldspar in all of the leucogranites have similar compositions ($An_{0.0–0.3}/Ab_{5.3–17.4}/Or_{82.4–94.7}$), with ~1–2 µg/g Be. Plagioclase in all types of leucogranites contain ~9–11 µg/g Be, and are predominantly euhedral and clearly zoned, with a composition trend of decreasing anorthite values from core to rim (Fig. 4). The plagioclase in biotite granite is oligoclase ($An_{14.0–23.2}/Ab_{74.7–84.7}/Or_{1.3–3.1}$). In two-mica granite, plagioclase varies from oligoclase to albite ($An_{2.6–18.2}/Ab_{80.5–96.1}/Or_{1.0–2.4}$). The plagioclase in muscovite and albite granites are almost all albite ($An_{1.3–10.9}/Ab_{87.4–97.7}/Or_{0.5–3.1}$). The Be contents of muscovite from different granites (~2 vol% in biotite granite) increase from 10 µg/g in biotite granite to 22 µg/g in albite granite. Biotite in the biotite- and two-mica granites contain a similar Be content, ~5–6 µg/g. Tourmaline is a common accessory mineral in all lithologies, and contains ~2–7 µg/g Be. According to the formulae (Novák et al. 1998; Burianek and Novák 2004; Ertl et al. 2016), tourmaline varies from fluor-dravite to fluor-schorl in biotite granite, and is fluor-schorl in the other evolved leucogranites and pegmatites (Supplemental Data 2.4).

Occurrence of beryl

Beryl is the only mineral in the Pusila pluton in which Be is an essential constituent, and its abundance increases from two-mica granite to pegmatite. The ubiquitous occurrence of beryl in the two-mica granite is reported for the first time in a relatively unevolved type of granite. Small beryl crystals about 50–100 μm across are commonly dispersed, among rock-forming minerals in the leucogranites (Figs. 5a–5c; Supplemental Fig. S2). In pegmatite, beryl crystals can be identified in outcrops (Fig. 2j), and typically form well-developed, euhedral, hexagonal columns that are light cyan in color. The petrographic evidence, e.g., subhedral–euhedral granular textures (Figs. 5a–5c), indicate that beryl from the Pusila leucogranites is of magmatic origin.

Beryl chemistry

Beryl, ideally $Be_3Al_2Si_6O_{18}$, contains trace elements, including Fe and Mg substituting for octahedral Al, Li substituting for tetrahedral Be, and Cs, Na, K and Ca as ring channel constituents. Overall, trace elements in beryl vary by 1–2 orders of magnitude from the two-mica granite to pegmatite: Na and Li increase and Fe and Mg decrease with increasing Cs (Fig. 6a; Supplemental Fig. S3; Supplemental Data 2.1). Moreover, the beryl in the Pusila pluton show continuous, gradually decreasing Na/Li and slightly decreasing Mg/Fe, coincident with a strong increase of the Cs/Na ratio (Figs. 6b–6c), which are also positively correlated with increasing Rb/Sr ratios of whole rock (reflected by the symbol size and border color on Fig. 6).

DISCUSSION

Fertile source providing the initial Be enrichment

The enrichment of Be and other critical elements in granitic melt is mainly controlled by the magma source, the saturation of key accessory minerals, mineral melt partition coefficients and extreme fractionation during crystallization (London 2008). There is a consensus that high to extremely high Be contents > 200 µg/g, which reflects critical element mineralization, is associated with strongly fractionated granites or their equivalents (e.g., rhyolite, aplite, pegmatite, etc.).

In the Pusila pluton, the high abundance of beryl has been observed not only in the highly evolved albite granite and pegmatite, but interestingly also in the moderately evolved two-mica granite and muscovite granite. It is not likely that a high degree of fractionation is the only factor needed to attain beryl saturation. Instead, a source relatively enriched in Be appears to be of first-order importance.

The average Be value is generally ~3–4 µg/g for biotite granites, and 5–10 µg/g for two-mica granites (Hörmann 1978; Taylor and McLennan 1985; Charoy 1999; Trueman and Sabey 2014; Foley et al. 2017, and others in Table 2). Abundance of Be in the Pusila biotite granite is as high as ~7 µg/g Be, and in the two-mica granite, up to ~22 µg/g Be, which are higher than the average values for comparable rocks worldwide (Fig. 7). Thus, the initial magma of the Pusila leucogranite was likely already enriched in Be, interpreted to have been a consequence of a source relatively enriched in Be. The principal sources for the granites that are fractionated to give beryl-bearing pegmatites are clay-rich marine sediments, e.g., shale, or their mica-rich metamorphic equivalents (London 2008). The Himalayan leucogranites have a

peraluminous composition and are considered to have originated from melting of the GHS (e.g., pelite, granitic gneiss; Harris et al. 2000; Hopkinson et al. 2019; Wu et al. 2020). The GHS gneisses contain ~4–6 µg/g Be (Table 3), that is about twice the mean Be concentration in pelitic rocks worldwide (~2–3 µg/g, Table 3; Grew 2002; Grew et al. 2006) and nearly 3 times the average Be concentration in the upper continental crust (2.1 µg/g, Rudnick and Gao 2014). Therefore, the pelitic and granitic gneisses in the GHS that melted to give the Pusila leucogranites were an effective source of Be for the initial melts.

This possibility has been investigated by modeling partial melting, where both batch melting and fractional melting are being considered (Harris and Inger 1992):

Firstly batch melting equation: $C_l/C_o = 1/[(D_o–PF)+F]$,

Secondly fractional melting equation: $C_l/C_o = (1/F)\ [1–(1–PF/D_o)^{1/P}]$.

D_o: Bulk distribution coefficient of a given trace element at the onset of melting;

C_o: Weight concentration of a trace element in the original unmelted solid;

C_l: Weight concentration of a trace element in melt;

P: Bulk distribution coefficient of minerals which make up a melt;

F: Weight fraction of melt relative to original parent.

Partial melting was modeled using a muscovite-biotite schist (MBS, Patiño Douce and Harris 1998) as the initial mineral assemblage, which is nearly identical to the most widespread mineral assemblage in GHS gneisses at Pusila. The Be partition coefficients for modeling partial melting are given in Table 4. It is estimated that ~30% partial melting of the gneiss would have generated a biotite granite melt with 6–7

μg/g Be (Table 4). The GHS gneisses, and leucogranites that constituting the Pusila pluton, were identified as cordierite-free. Granitic magmas that originate from cordierite-bearing protoliths will not achieve beryl saturation at any point in their evolution, owing to the very high compatibility of Be in cordierite (Evensen and London, 2002; London, 2008). Among the common minerals in the pelitic and granitic gneisses of the GHS, the white micas are expected to have the highest Be concentrations, which could reach 10 μg/g (Grew, 2002; Ryan, 2002). Melting of white mica would lead to its being nearly completely decomposed over a narrow range of temperature (Acosta-Vigil et al., 2003), liberating thereby their trace elements including Be to the magma, which results in a relatively high initial Be concentration in the magma.

Sequential fractionation model of magmatic evolution

Generation of granitic magmas with increasing contents of incompatible elements is commonly attributed to fractional crystallization, which can eventually lead to the enrichment of critical elements in leucogranites and pegmatites (e.g., Raimbault et al. 1995; Breiter et al. 1997; Linnen et al. 2012; London and Morgan 2012). From the biotite granite to pegmatite, some whole-rock compositional parameters are obviously indicative of fractionation, including the decrease in Ti and REE contents, and increase in Rb/Sr and decrease in Zr/Hf and Nb/Ta ratios (Fig. 3; Supplemental Fig. S1; Supplemental Data 1.1). The trends of Na-Li-Cs enrichment and Fe-Mg depletion of beryl in the Pusila pluton are similar to well documented trends of beryl in rare-element pegmatites worldwide (e.g., Aurisicchio et al. 1988;

Černý 2002). Chemical trends resulting from magmatic fractionation are reflected in changes of beryl chemistry, including the decreasing Na/Li and Mg/Fe, and increasing Cs/Na ratios (Fig. 6). Tourmaline and muscovite show continuous trends of increasing F/(F+OH) and decreasing Mg/(Mg+Fe) ratios (Supplemental Fig. S4). These geochemical and mineralogical characteristics of the Pusila leucogranitic rocks record magmatic differentiation with progressive fractionation.

The equation for Rayleigh fractionation is: $C_L = C_O F^{D-1}$, where the element concentrations in residual liquids (C_L) can be related to a parental melt (C_O), the F is the fraction of liquid remaining, and D is the distribution coefficient between liquid and solids, determined by the partition coefficient for each mineral phase weighted according to the phase proportions (Table 5). In this study, our modeling of Rb and Sr has a reasonable fit with the observed data (Fig. 8a). Melt compositions similar to two-mica granite could be achieved by 40–50% fractional crystallization of the biotite granite melt, and subsequent fractionation could successively produce the muscovite granite, albite granite and pegmatite compositions. These, in turn, provides estimates for the degree of crystallization (1 - F) for each of the leucogranites, which were then used to model the Cs concentration at each stage of melt. The calculated Cs concentrations agree reasonably well with the observed data (Fig. 8b). In the model for Be, ~50% fractional crystallization of biotite granite melt is needed to generate the two-mica granite composition (Fig. 8c), in agreement with the results for Rb, Sr, and Cs.

However, this model failed to replicate the observed data for the more evolved

albite granite and pegmatite. We attribute this failure to saturation of the melt with beryl, at which point beryllium is no longer an incompatible constituent of the melt. Instead, whole-rock Be compositions are controlled by the buffering action of beryl, which is crystallizing out from the melt. In contrast, a saturating phase for Cs (e.g., pollucite, London 2019) did not crystallize out in the Pusila leucogranites. Thus, Cs remained incompatible during evolution of the leucogranite and Rayleigh fractionation modeling works well for Cs. Similarly, we expect Rayleigh fractionation would work well for other elements that remained incompatible. Beryllium partitioned into rock-forming minerals, notably white mica and plagioclase, together with the Be contained in beryl crystallizing from the melt, add up to give the total amount Be originally in the leucogranite. The Be partition coefficients of whole rock were revised by considering the accumulated accessary beryl (Table 6). Although the crystallization of beryl consumed Be from the initial melt, the differentiation of the two-mica granite and muscovite granite still greatly increase the Be concentration in the residual melt, as a consequence of the low bulk Be partition coefficients ($D_{Be\ (rock/melt)}$ = 0.25 – 0.30, Table 7). It is noteworthy that although Be and Cs are progressively enriched in melt by fractionation, their enrichment processes are different during magma evolution, owing to differences in their bulk partition coefficients.

Delayed beryl crystallization and continuous beryl mineralization

Theoretically, fractionation could generate the initial beryl saturation as seen in the two-mica granite, but the continuously fractionated and Be-saturated melt should

329 result in progressively lower Be contents with evolution (increasing ASI and
330 decreasing T, Evensen et al. 1999). However, this is contradictory to the case in Pusila
331 where Be contents progressively increase with differentiation since the abundance of
332 beryl is higher in the leucogranites. Thus, it suggests that fractionation by itself cannot
333 explain the continuous increase of the Be content in the Pusila leucogranite pluton.

334 As the behavior of Be can shift from incompatible to compatible owing to the
335 beryl crystallization, it is crucial to determine the precise point where beryl became
336 saturated. Beryl crystals in two-mica granite and muscovite granite are mostly
337 characterized by the texture of subhedral and interstitial grains among rock-forming
338 minerals (Figs. 5a–5b; Supplemental Fig. S2). This petrographic feature indicates the
339 crystallization of beryl just at the final stage of granite solidification. Considering the
340 overlapping compositions between rims of plagioclase in the leucogranite and cores
341 of plagioclase in the subsequent leucogranite (Fig. 4), the removal of fractionated melt
342 seems incomplete, resulting in a certain amount of residual melt having been left
343 behind, which then crystallized *in situ*. This *in situ* crystallization of residual melt
344 after incomplete separation of the residual melt can be referred to as "Delayed
345 crystallization". At the onset of delayed crystallization, abundant crystallization of
346 rock-forming minerals led to the enrichment of Be due to their low partition
347 coefficients for Be in these minerals (Evensen and London 2002; Table 5). The lower
348 temperature of interstitial melt decreases beryl solubility (Evensen et al. 1999), which
349 also promoted the delayed crystallization of beryl in the residual melt. Thus, the term
350 "Delayed crystallization of beryl" is suggested to describe the process of Be

enrichment in the two-mica granite and muscovite granite (Fig. 9). The fractionated melt was then extracted and formed the albite granite near the top of the Pusila pluton, likely achieved by flow of melt away from the crystallization site (Sawyer 1987). As expected, this fractionated melt is beryl-saturated, and abundant euhedral beryl crystallized (C-I, in Fig. 9), and continued to grow as an accumulation phase (C-II, in Fig. 9).

The widespread occurrences of tourmaline in the Pusila pluton indicate that the melt had a high concentration of boron. Mineral chemistry of muscovite and especially tourmaline yielded high contents of F (Supplemental Data 2.2 and 2.4). In tourmaline, the homovalent substitution (OH) ↔ F at the O1 crystallographic site relates dravite or schorl to flour- dravite or schorl, respectively (Bosi et al. 2018). The melt of pegmatite contains the most abundant fluid and highest F content, which is recorded by the tourmaline chemistry, due to its sensitivity to the associated fluid (von Goerne et al. 1999, 2011). Evidently, the individual leucogranitic magma contained high amounts of fluid (H_2O, B, F), which increased during differentiation. It is interpreted that the fluid-rich melt had a low viscosity and density compared to the bulk melt and migrated upward (Bartels et al. 2015; Pollard 2021). Such highly evolved melts tend to sequester incompatible elements (Thomas and Davidson 2013), and in the case of Pusila, the fluid-rich melt attained extreme Be-Nb-Ta-Li enrichment (two stages of Li mineralization, including magmatic and hydrothermal stages; Liu et al. 2020), and continuous beryl crystallization (C-I) ultimately led to the formation of giant crystals in the pegmatites (C-II).

373 In conclusion, multiple processes need to be considered to interpret the whole
374 rock abundances of incompatible elements like Be. The continuous beryl
375 mineralization in Pusila leucogranites, with a progressive increase in whole rock Be
376 contents is illustrated by the continuous crystallization model (Fig. 9). The bulk melts
377 of the two-mica granite and muscovite granite were initially unsaturated in beryl, but
378 beryl crystallized from interstitial residual melts during delayed crystallization. The
379 fractionated melts formed albite granite and pegmatite, and their bulk melts were
380 beryl saturated, which resulted in the crystallization of abundant euhedral beryl.
381

382 ## IMPLICATIONS

383 Beryllium is a critical metal typically concentrated in highly fractionated granitic
384 rocks. The beryl mineralization in what appears to be a typical leucogranite pluton at
385 Pusila in the central Himalaya is a striking example of continuous Be mineralization.
386 (1) Beryl is the most common beryllium mineral (Grew and Hazen 2014), and is
387 ubiquitous at Pusila. The beryl compositions trend to Na-Li-Cs enrichment and Fe-Mg
388 depletion, and show continuous decreasing Na/Li and Mg/Fe, and increasing Cs/Na
389 ratios, which is positively correlated with increasing whole-rock Rb/Sr ratio. Mineral
390 chemistry characteristics above highlight the beryl as a monitor of magmatic
391 evolution processes from the earlier stage.
392 (2) The enrichments of Be and other critical elements are associated with
393 strongly fractionated granites or their equivalents. Despite the low to moderate
394 fractionation, the biotite- and two-mica granites contain unusually high Be contents,

indicative of an initial magma relatively enriched in Be. The gneisses of GHS, considered as the protolith, also show high Be abundances, which could be the source reservoir of Be. Therefore, a high degree of fractionation is likely not the only factor for Be saturation. A source relatively enriched in Be could effectively reduce the dependence on the degree of fractionation to concentrate Be sufficiently to reach saturation.

(3) This study reveals the differing behaviors of incompatible elements (e.g., Be, Cs) in melt. Once saturated, beryllium is no longer strictly incompatible owing to the beryl crystallization, and the Be concentrations would be concurrently controlled by multiple processes like fractional crystallization and the buffering action of beryl crystallizing out when saturation had been attained. This combination of processes could be applicable to other trace and incompatible elements.

(4) The term "delayed crystallization", describing the process of beryl crystallization at the late stage of granite solidification in two-mica granite and muscovite granite, is the crucial part of the continuous crystallization model. This continuous crystallization model reveals the evolutionary mechanisms of continuous Be mineralization with a progressive increase in whole rock Be contents, and concurrently could provide new insights into the enrichment processes of other critical metal elements, like Cs, Li, Zr, etc., which are commonly rare and incompatible in granitic melts.

ACKNOWLEDGMENTS AND FUNDING

This study was supported by the National Natural Science Foundation of China (Grant No.91855209), Second Comprehensive Scientific Investigation into Qinghai-Tibet Plateau (Grant No.2019QZKK0802), the scholarship from China Scholarship Council (File No.201906190151) to C.L., and the Fundamental Research Funds for the Central Universities (DLTD2014). We sincerely thank Wen-Lan Zhang, Huan Hu, and Juan Li from State Key Laboratory for Mineral Deposits Research for their technical assistance with EMPA, LA-ICPMS, and SEM analyses. We sincerely thank the two reviewers, Gerhard Franz, and Milan Novák for their constructive comments. We also wish particularly to thank the Associate Editor, Edward S. Grew for bringing his considerable expertise with patience to bear on important details.

REFERENCES CITED

Acosta-Vigil, A., London, D., Morgan VI, G.B. and Dewers, T.A. (2003) Solubility of excess alumina in hydrous granitic melts in equilibrium with peraluminous minerals at 700–800 °C and 200 MPa, and applications of the aluminum saturation index. Contributions to Mineralogy and Petrology, 146, 100–119, https://doi.org/10.1007/s00410-003-0486-6.

Aikman, A.B., Harrison, T.M. and Hermann, J. (2012) The origin of Eo- and Neo-himalayan granitoids, Eastern Tibet. Journal of Asian Earth Sciences, 58, 143–157, https://doi.org/10.1016/j.jseaes.2012.05.018.

Aurisicchio, C., Fioravanti, G., Grubessi, O. and Zanazzi, P.F. (1988) Reappraisalof the crystal chemistry of beryl. American Mineralogist, 73, 826–837.

Ayres, M., Harris, N. and Vance, D. (1997) Possible constraints on anatectic melt residence times from accessory mineral dissolution rates: an example from Himalayan leucogranites. Mineralogical Magazine, 61, 29–36, https://doi.org/10.1180/minmag.1997.061.404.04.

Bartels, A., Behrens, H., Holtz, F. and Schmidt, B. (2015) The effect of lithium on the viscosity of pegmatite forming liquids. Chemical Geology, 410, 1–11, https://doi.org/10.1016/j.chemgeo.2015.05.011.

Bea, F., Pereira, M.D., Corretgé, L.G. and Fershtater, G.B. (1994) Differentiation of strongly peraluminous, perphosphorus granites: The pedrobernardo pluton, central Spain. Geochimica et Cosmochimica Acta, 58, 2609–2627, https://doi.org/10.1016/0016-7037(94)90132-5.

Beus, A.A. (1966) Geochemistry of Beryllium and genetic types of Beryllium deposits. Page, L.R., Lachman, F. and Harrison, R.K., eds. San Francisco and London, 401 p. The Geochemical Society, W. H. Freeman and Company.

Bosi, F., Naitza, S., Skogby, H., Secchi, F., Conte, A.M., Cuccuru, S., Hålenius, U.,

De La Rosa, N., Kristiansson, P., Charlotta Nilsson, E.J., Ros, L. and Andreozzi, G.B. (2018) Late magmatic controls on the origin of schorlitic and foititic tourmalines from late-Variscan peraluminous granites of the Arbus pluton (SW Sardinia, Italy): Crystal-chemical study and petrological constraints. Lithos, 308–309, 395–411, https://doi.org/10.1016/j.lithos.2018.02.013.

Breiter, K., Sokolová, M. and Sokol, A. (1991) Geochemical specialization of the tin-bearing granitoid massifs of NW Bohemia. Mineralium Deposita, 26, 298–306, https://doi.org/10.1007/BF00191077.

Breiter, K., Frýda, J., Seltmann, R. and Thomas, R. (1997) Mineralogical Evidence for Two Magmatic Stages in the Evolution of an Extremely Fractionated P-rich Rare-metal Granite: the Podlesí Stock, Krušné Hory, Czech Republic. Journal of Petrology, 38 (12), 1723–1739, https://doi.org/10.1093/petroj/38.12.1723.

Breaks, F.W. and Moore, J.M. (1992) The Ghost Lake Batholith, Superior Province of northwestern Ontario: a fertile, S-type, peraluminous granite - rare-element pegmatite system. The Canadian Mineralogist, 30, 835–875.

Breaks, F.W. and Tindle, A.G. (2001) Rare-element mineralization of the Separation Lake area, northwest Ontario: characteristics of a new discovery of complex-type, petalite-subtype, Li-Rb-Cs-Ta pegmatite. Industrial Minerals in Canada, 53, 159–178.

Buriánek, D. and Novák, M. (2004) Morphological and compositional evolution of tourmaline from nodular granite at Lavičky near Velké Meziříčí, Moldanubicum, Czech Republic. Journal of the Czech Geological Society, 49, 81–90.

Černý, P. (2002) Mineralogy of Beryllium in Granitic Pegmatites, in Beryllium: Mineralogy, Petrology, and Geochemistry. Ribbe, P.H., ed., Reviews in Mineralogy and Geochemistry, 405–444. Blacksburg, Virginia, https://doi.org/10.2138/rmg.2002.50.10.

Černý, P. and Ercit, T.S. (2005) The classification of granitic pegmatites revisited. The Canadian Mineralogist, 43, 2005–2006, https://doi.org/10.2113/gscanmin.43.6.2005.

Chakhmouradian, A.R., Smith, M.P. and Kynicky, J. (2014) From “strategic” tungsten to “green” neodymium: A century of critical metals at a glance. Ore Geology Reviews, 64, 455–458, https://doi.org/10.1016/j.oregeorev.2014.06.008.

Charoy, B. (1999) Beryllium speciation in evolved granitic magmas: phosphates versus silicates. European Journal of Mineralogy, 11, 135–148, https://doi.org/10.1127/ejm/11/1/0135.

Chen, G.H., Shu, L.S., Shu, L.M., Zhang, C. and Ou-Yang, Y.P. (2016) Geological characteristics and mineralization setting of the Zhuxi tungsten (copper) polymetallic deposit in the Eastern Jiangnan Orogen. Science China Earth Sciences, 59 (4), 803–823, https://doi.org/10.1007/s11430-015-5200-9.

Chen, W., Chen, B. and Sun, K.K. (2018) Petrogenesis of the Zengjialong highly differentiated granite in the Pengshan Sn-polymetallic ore field, Jiangxi Province (in Chinese with English abstract). Geochimica, 47, 554–574, https://doi.org/10.19700/j.0379-1726.2018.05.008.

Drake, M.J. and Weill, D.F. (1975) Partition of Sr, Ba, Ca, Y, Eu2+, Eu3+, and other REE between plagioclase feldspar and magmatic liquid: an experimental study. Geochimica et Cosmochimica Acta, 39, 689–712, https://doi.org/10.1016/0016-7037(75)90011-3.

Ertl, A., Kolitsch, U., Dyar, M.D., Meyer, H.P., Rossman, G.R., Henry, D.J., Prem, M., Ludwig, T., Nasdala, L., Lengauer, C.L., Tillmanns, E. and Niedermayr, G. (2016) Fluor-schorl, a new member of the tourmaline supergroup, and new data on schorl from the cotype localities. European Journal of Mineralogy, 28, 163–177, https://doi.org/10.1127/ejm/2015/0027-2501

Evensen, J.M., London, D. and Wendlandt, R.F. (1999) Solubility and stability of beryl in granitic melts. American Mineralogist, 84, 733–745, https://doi.org/10.2138/am-1999-5-605.

Evensen, J.M. and London, D. (2002) Experimental silicate mineral/melt partition coefficients for beryllium and the crustal Be cycle from migmatite to pegmatite. Geochimica et Cosmochimica Acta, 66 (12), 2239–2265, https://doi.org/10.1016/S0016-7037(02)00889-X.

Foley, N.K., Jaskula, B.W., Piatak, N.M. and Schulte, R.F. (2017) Beryllium, *in* Critical mineral resources of the United States: economic and environmental geology and prospects for future supply. Schulz, K.J., DeYoung, J.H., Seal, R.R. and Bradley, D.C., eds., U.S. Geological Survey: Reston, Virginia, chapter E, https://doi.org/10.3133/pp1802E.

Grew, E.S. (2002) Beryllium in Metamorphic Environments (emphasis on aluminous compositions), *in* Beryllium: Mineralogy, Petrology, and Geochemistry. Ribbe, P.H., ed. Reviews in Mineralogy and Geochemistry, 487–549. Blacksburg, Virginia, https://doi.org/10.2138/rmg.2002.50.12.

Grew, E.S., Yates, M.G., Shearer, C.K., Hagerty, J.J., Sheraton, J.W. and Sandiford, M. (2006) Beryllium and Other Trace Elements in Paragneisses and Anatectic Veins of the Ultrahigh-Temperature Napier Complex, Enderby Land, East Antarctica: the Role of Sapphirine. Journal of Petrology, 47 (5), 859–882, https://doi.org/10.1093/petrology/egi098.

Grew, E.S. and Hazen, R.M. (2014) Beryllium mineral evolution. American Mineralogist, 99, 999–1021. https://doi.org/10.2138/am.2014.4675.

Harris, N. and Inger, S. (1992) Trace element modelling of pelite-derived granites. Contributions to Mineralogy and Petrology, 110, 46–56, https://doi.org/10.1007/BF00310881.

Harris, N., Vance, D. and Ayres, M. (2000) From sediment to granite: Timescales of anatexis in the upper crust. Chemical Geology, 162, 155–167, https://doi.org/10.1016/S0009-2541(99)00121-7.

Hopkinson, T., Harris, N., Roberts, N.M.W., Warren, C.J., Hammond, S. and Spencer, C.J. (2019) Evolution of the melt source during protracted crustal anatexis: An example from the Bhutan Himalaya. Geology, 48 (1), 87–91, https://doi.org/10.1130/G47078.1.

Hörmann, P.K. (1978) Beryllium: Handbook of Geochemistry II/1. Wedepohl, K. H., ed., 1–6. Springer, Berlin.

Icenhower, J. and London, D. (1995) An experimental study of element partitioning among biotite, muscovite, and coexisting peraluminous silicic melt at 200 MPa (H_2O). American Mineralogist, 80, 1229–1251, https://doi.org/10.2138/am-1995-11-1213.

Icenhower, J. and London, D. (1996) Experimental partitioning of Rb, Cs, Sr, and Ba between alkali feldspar and peraluminous melt. American Mineralogist, 81, 719–734, https://doi.org/10.2138/am-1996-5-619.

Le Fort, P., Cuney, M., Deniel, C., France-Lanord, C., Sheppard, S.M.F., Upreti, B.N. and Vidal, P. (1987) Crustal generation of the Himalayan leucogranites. Tectonophysics, 134, 39–57, https://doi.org/10.1016/0040-1951(87)90248-4.

Linnen, R.L., Lichtervelde, M.V. and Černý, P. (2012) Granitic Pegmatites as Sources of Strategic Metals. Elements, 8, 275–280, https://doi.org/10.2113/gselements.8.4.275.

Liu, Y.S., Hu, Z.C., Gao, S., Günther, D., Xu, J., Gao, C.G. and Chen, H.H. (2008) In situ analysis of major and trace elements of anhydrous minerals by LA-ICP-MS without applying an internal standard. Chemical Geology, 257, 34–43, https://doi.org/10.1016/j.chemgeo.2008.08.004.

Liu, C., Wang, R.C., Wu, F.Y., Xie, L., Liu, X.C., Li, X.K., Yang, L. and Li, X.J. (2020) Spodumene pegmatites from the Pusila pluton in the higher Himalaya, South Tibet: Lithium mineralization in a highly fractionated leucogranite batholith. Lithos, 358–359, 105421, https://doi.org/10.1016/j.lithos.2020.105421.

London, D. (2015) Reading Pegmatites: Part 1—What Beryl Says. Rock & Minerals, 90 (2), 138–151, https://doi.org/10.1080/00357529.2014.949173.

London, D. (2019) Reading Pegmatites: Part 5—What Pollucite Says. Rock & Minerals, 94 (5), 420–427, https://doi.org/10.1080/00357529.2019.1619135.

London, D. (2008) Pegmatites. Martin, R.F. ed. The Canadian Mineralogist, 347 p. Canada, Special Publication 10.

London, D. and Evensen, J.M. (2002) Mineralogy of Beryllium in Granitic Pegmatites, in Beryllium: Mineralogy, Petrology, and Geochemistry, Ribbe, P.H., ed., Reviews in Mineralogy and Geochemistry, 445–486. Blacksburg, Virginia,

https://doi.org/10.2138/rmg.2002.50.11.

London, D. and Morgan, G.B. (2012) The Pegmatite Puzzle. Elements 8, 263–268, https://doi.org/10.2113/gselements.8.4.263.

Long, P.E. (1978) Experimental determination of partition coefficients for Rb, Sr, and Ba between alkali feldspar and silicate liquid. Geochimica et Cosmochimica Acta, 42, 833–846, https://doi.org/10.1016/0016-7037(78)90096-0.

Lowell, G.R. and Young, G.J. (1999) Interaction between coeval mafic and felsic melts in the St. Francois Terrane of Missouri, USA. Precambrian Research, 95, 69–88, https://doi.org/10.1016/S0301-9268(98)00127-2.

Montel, J.M. (1993) A model for monazite/melt equilibrium and application to the generation of granitic magmas. Chemical Geology, 110, 127–146, https://doi.org/10.1016/0009-2541(93)90250-M.

Norton, J.J. and Redden, J.A. (1990) Relations of zoned pegmatites to other pegmatites, granite, and metamorphic rocks in the southern Black Hills, South Dakota. American Mineralogist, 75, 631–655.

Novák, M., Selway, J.B. and Houzar, S. (1998) Potassium-bearing, fluorine-rich tourmaline from metamorphosed fluorite layer in leucocratic orthogneiss at Nedvědice, Svratka Unit, western Moravia. Journal of the Czech Geological Society, 43, 37–44.

Patiño Douce, A.E. and Harris, N. (1998) Experimental Constraints on Himalayan Anatexis. Journal of Petrology. 39, 689–710, https://doi.org/10.1093/petroj/39.4.689.

Pollard, P.T. (2021) The Yichun Ta-Sn-Li Deposit, South China: Evidence for Extreme Chemical Fractionation in F-Li-P-Rich Magma. Economic Geology, 116 (2), 453–469, https://doi.org/10.5382/econgeo.4801.

Qi, L., Hu, J. and Gregoire, D.C. (2000) Determination of trace elements in granites by inductively coupled plasma mass spectrometry. Talanta, 51, 507–513, https://doi.org/10.1016/S0039-9140(99)00318-5.

Raimbault, L., Cuney, M., Azencott, C., Duthou, J.L. and Joron, J.L. (1995) Geochemical evidence for a multistage magmatic genesis of Ta-Sn-Li mineralization in the granite at Beauvoir, French Massif Central. Economic Geology, 90, 548–576, https://doi.org/10.2113/gsecongeo.90.3.548.

Ramírez, J.A. and González-Menéndez, L.A. (1999) Geochemical Study of Two Peraluminous Granites from South-Central Iberia: The Nisa-Albuquerque and Jalama Batholiths. Mineralogical Magazine, 63, 85–104, https://doi.org/10.1180/minmag.1999.063.1.09.

Ramírez, J.A. and Grundvig, S. (2000) Causes of geochemical diversity in peraluminous granitic plutons: the Jálama pluton, Central-Iberian Zone (Spain and Portugal). Lithos, 50, 171–190,

https://doi.org/10.1016/S0024-4937(99)00047-X.

Rudnick, R., and Gao, S. (2014) Composition of the continental crust, in The Crust, Rudnick R.L., Holland, H.D. and Turekian, K.K., eds. Treatise on Geochemistry, 3, 1–64. Elsevier–Pergamon, Oxford, https://doi.org/10.1016/B978-0-08-095975-7.00301-6.

Ryan, J.G. (2002) Trace-Element Systematics of Beryllium in Terrestrial Materials, in Beryllium: Mineralogy, Petrology, and Geochemistry. Ribbe, P.H., ed. Reviews in Mineralogy and Geochemistry, 121–145. Blacksburg, Virginia, https://doi.org/10.2138/rmg.2002.50.3.

Sawyer, E. (1987) The Role of Partial Melting and Fractional Crystallization in Determining Discordant Migmatite Leucosome Compositions. Journal of Petrology, 28, 445–473, https://doi.org/10.1093/petrology/28.3.445.

Scaillet, B., France-Lanord, C. and Le Fort, P. (1990) Badrinath-Gangotri plutons (Garhwal, India): petrological and geochemical evidence for fractionation processes in a high Himalayan leucogranite. Journal of Volcanology and Geothermal Research, 44, 163–188, https://doi.org/10.1016/0377-0273(90)90017-A.

Sovacool, B.K., Ali, S.H., Bazilian, M., Radley, B., Nemery, B., Okatz, J. and Mulvaney, D. (2020) Sustainable minerals and metals for a low-carbon future. Science, 367, 30–33, https://doi.org/10.1126/science.aaz6003.

Taylor, S.R., and McLennan, S.M. (1985) The continental crust: Its composition and evolution; an examination of the geochemical record preserved in sedimentary rocks, 312 p. United Kingdom, Blackwell Scientific Publishing.

Thomas, R. and Davidson, P. (2013) The missing link between granites and granitic pegmatites. Journal of Geosciences, 58, 183–200, https://doi.org/10.3190/jgeosci.135.

Tian, E.N., Wang, R.C., Xie, L., Zhang, W.L., Che, X.D. and Zhang, R.Q. (2020) Mineralogy and geochemistry of the newly discovered Late Mesozoic granite-pegmatite and associated Sn-Nb-Ta-Be mineralization in the Miao'ershan-Yuechengling composite batholith, northern Guangxi, South China. Journal of Asian Earth Sciences, 190, 104149, https://doi.org/10.1016/j.jseaes.2019.104149.

Trueman, D.L., and Sabey, P. (2014) Beryllium, in Critical Metals Handbook, Gunn, G., ed., British Geological Survey, American Geophysical Union, Wiley, 99–119. Nottingham, UK.

von Goerne, G., Franz, G. and Wirth, R. (1999) Hydrothermal synthesis of large dravite crystals by the chamber method. European Journal of Mineralogy, 11 (6), 1061–1077, https://doi.org/10.1127/ejm/11/6/1 061.

von Goerne, G., Franz, G. and van Hinsberg, V. (2011) Experimental determination of

649 Na-Ca distribution between tourmaline and fluid in the system
650 CaO-Na_2O-MgO-Al_2O_3-SiO_2-B_2O_3-H_2O. The Canadian Mineralogist, 49 (1),
651 137–152, https://doi.org/10.3749/canmin.49.1.137.
652 Watson, E.B., and Harrison, T.M. (1983) Zircon saturation revisited: temperature and
653 composition effects in a variety of crustal magma types. Earth and Planetary
654 Science Letters, 64, 295–304, https://doi.org/10.1016/0012-821X(83)90211-X.
655 Wang, R.C., Wu, F.Y., Xie, L., Liu, X.C., Wang, J.M., Yang, L., Lai, W. and Liu, C.
656 (2017) A preliminary study of rare-metal mineralization in the Himalayan
657 leucogranite belts, South Tibet. Science China Earth Science, 60 (9), 1655–1663,
658 https://doi.org/10.1007/s11430-017-9075-8.
659 Wu, F.Y., Liu, X.C., Liu, Z.C., Wang, R.C., Xie, L., Wang, J.M., Ji, W.Q., Yang, L.,
660 Liu, C., Khanal, G.P. and He, S.X. (2020) Highly fractionated Himalayan
661 leucogranites and associated rare-metal mineralization. Lithos, 352–353, 105319,
662 https://doi.org/10.1016/j.lithos.2019.105319.
663 Xiang, L., Romer, R.L., Glodny, J., Trumbull, R.B. and Wang, R. C. (2020) Li and B
664 isotopic fractionation at the magmatic-hydrothermal transition of highly evolved
665 granites. Lithos, 376–377,105753, https://doi.org/10.1016/j.lithos.2020.105753.
666 Yang, L. (2020) Research on the relationship between anatexis and petrogenesis of
667 leucogranite in the Himalayan orogenic belt, 256 p. Ph.D. thesis, Beijing,
668 Institute of Geology and Geophysics Chinese Academy of Sciences.
669 Zaraisky, G.P., Aksyuk, A.M., Devyatova, V.N., Udoratina, O.V. and Chevychelov,
670 V.Y. (2009) The Zr/Hf ratio as a fractionation indicator of rare-metal granites.
671 Petrology, 17, 25–45, https://doi.org/10.1134/S0869591109010020.
672 Zhang, S.T. Ma, D.S., Lu, J.J., Zhang, R.Q., Cai, Y. and Ding, C.C. (2016)
673 Geochronology, Hf Isotopic Compositions and Geochemical Characteristics of
674 the Pingying Granite Pluton in Northern Guangxi, South China, and Its
675 Geological Significance (in Chinese with English abstract). Geological Journal
676 of China Universities, 22, 92–104,
677 https://doi.org/10.16108/j.issn1006-7493.2015025.
678 Zhang, F., Wang, Y.B. and Yang, D.T. (2020) Zircon U–Pb, O isotope, and
679 geochemistry study of the early Palaeozoic granitic gneiss in the Dinggye district,
680 central Himalaya: Implications for the early Palaeozoic orogenic event along the
681 northern margin of Gondwana. Geological Journal, 55, 439–456,
682 https://doi.org/10.1002/gj.3383.
683 Zhu, D.C. Wang, Q., Zhao, Z.D., Chung, S.L., Cawood, P.A., Niu, Y.L., Liu S.A., Wu,
684 F.Y. and Mo, X.X. (2015) Magmatic record of India-Asia collision. Scientific
685 Reports, 5, 1–9, https://doi.org/10.1038/srep14289.

686

FIGURE CAPTIONS

Figure 1. Geological setting of the Pusila pluton. (a). Distribution of the Himalayan leucogranites (after Wu et al., 2020). **(b)** Geological map of the Pusila pluton. **(c)** Schematic diagram of the Pusila pluton. The approximate width at the base of Pusila pluton is ~20 kilometers.

Figure 2. Outcrop photos of the Pusila pluton and photomicrographs of the leucogranites and pegmatites. **(a, b)** Outcrop and mineral constituents of the biotite granite. **(c, d)** Outcrop and mineral constituents of the two-mica granite. **(e, f)** Outcrop and mineral constituents of the muscovite granite. **(g, h)** Outcrop and mineral constituents of the albite granite. **(i)** Outcrop of the spodumene (-petalite) pegmatite dikes. **(j, k)** Specimen photo and characteristic mineral constituents of the pegmatite. Abbreviations: Kfs = K-feldspar; Pl = plagioclase; Oli = oligoclase; Ab = albite; Qtz = quartz; Mus = muscovite; Bt = biotite; Spd = spodumene; Brl = beryl; Tur = tourmaline.

Figure 3. Co-variation of whole-rock trace elements in the Pusila leucogranites. **(a)** Rb/Sr versus TiO_2. **(b)** Rb/Sr versus Be. **(c)** Comparison between zircon- and monazite-saturation temperatures.

Figure 4. Box-plot for An (anorthite) values of Plagioclase in leucogranites. Pl: Plagioclase; Biotite G: Biotite granite; Two-mica G: Two-mica granite; Muscovite G:

Muscovite granite; Albite G: Albite granite.

Figure 5. Occurrence of beryl (BSE images). (a) Small beryl crystals in two-mica granite. **(b)** Subhedral beryl crystals interstitial to rock-forming minerals in muscovite granite. **(c)** Euhedral or subhedral beryl crystals in albite granite. Abbreviations: Brl = beryl; Kfs = K-feldspar; Pl = plagioclase; Ab = albite; Qtz = quartz; Mus = muscovite; Bt = biotite.

Figure 6. Composition of beryl. (a) Covariance Cs (μg/g) versus Li(μg/g). **(b)** Na/Li (μg/g) versus Cs (μg/g). **(c)** Cs/Na (apfu) versus Mg/Fe (apfu).

Figure 7. Comparison of Be contents between Pusila leucogranites and other biotite- and two-mica granites worldwide. 2-Mica G = two-mica granite; Bt G = biotite granite.

Figure 8. Modeling of Rayleigh fractionation in Pusila leucogranites and pegmatites. (**a)** Rb versus Sr variation diagram. **(b)** Rb/Sr versus Cs variation diagram. **(c)** Rb/Sr versus Be variation diagram. The mean composition of biotite granites was used as the starting composition.

Figure 9. Schematic continuous crystallization model illustrating the continuous beryl crystallization in the Pusila pluton. C-I: Fractional crystallization in bulk melt;

C-II: Delayed crystallization in residual interstitial melt after fractionation.

TABLE CAPTIONS

Table 1. Beryllium reservoirs in Pusila leucogranites.

Table 2. Beryllium contents in biotite granites and two-mica granites worldwide.

Table 3. Beryllium contents in gneisses and pelitic rocks worldwide.

Table 4. Modeled Be content after partial melting.

Table 5. Rb-Sr-Be-Cs partition coefficients of main minerals for modeling Rayleigh fractionation.

Table 6. Beryllium partition coefficients of beryl.

Table 7. Beryllium partition coefficients of whole rock (including beryl).

SUPPLEMENTAL ITEMS

Item S1: Supplemental Figures.

Supplemental Figure S1. Co-variation of whole-rock trace elements in the Pusila leucogranites. (a) Rb/Sr versus Zr/Hf. **(b)** Rb/Sr versus Nb/Ta. **(c)** Rb/Sr versus distance from the first biotite granite sampling point.

Supplemental Figure S2. Occurrence of beryl. (a–d) Small beryl crystals in two-mica granite (**a, b** EDS maps; **c, d** BSE images). **(e)** Subhedral beryl crystals interstitial to rock-forming minerals in muscovite granite (BSE image). **(f)** Euhedral or subhedral beryl crystals in albite granite (BSE image). Abbreviations: Brl = beryl; Kfs = K-feldspar; Pl = plagioclase; Ab = albite; Qtz = quartz; Mus = muscovite; Bt =

753 biotite.

754 **Supplemental Figure S3. Composition of beryl. (a)** Covariance Cs (µg/g) versus Na

755 (µg/g). **(b)** Covariance Cs (µg/g) versus Fe + Mg (µg/g).

756 **Supplemental Figure S4. Composition of tourmaline and muscovite. (a)**

757 Covariance F/(F+OH) (apfu) versus Mg/(Mg+Fe) (apfu) in compositions of

758 tourmaline. **(b)** Covariance F/(F+OH) (apfu) versus Mg/(Mg+Fe) (apfu) in

759 compositions of muscovite.

760

761 **Item S2: Additional Information on Parting Melting.**

762

763 ## SUPPLEMENTAL DATA

764 **Supplemental Data 1: Whole rock geochemistry.**

765 Sheet 1.1 Whole rock geochemistry of leucogranites and pegmatites.

766

767 **Supplemental Data 2: Minerals chemistry.**

768 Sheet 2.1 EMPA and LA-ICPMS analyses of beryl.

769 Sheet 2.2 Representative EMPA and LA-ICPMS analyses of micas.

770 Sheet 2.3 Representative EMPA and LA-ICPMS analyses of feldspars.

771 Sheet 2.4 EMPA and LA-ICPMS analyses of tourmaline.

772 Sheet 2.5 EMPA and LA-ICPMS analyses of quartz.

773

774 **Supplemental Data 3: Statistics.**

775 Sheet 3.1 Statistics of Be contents in biotite granites and two-mica granites
776 worldwide.
777 Sheet 3.2 Statistics of Be contents in pelitic rocks in Himalaya.
778 Sheet 3.3 Statistics of Be contents in pelitic rocks worldwide.

Figure 1.

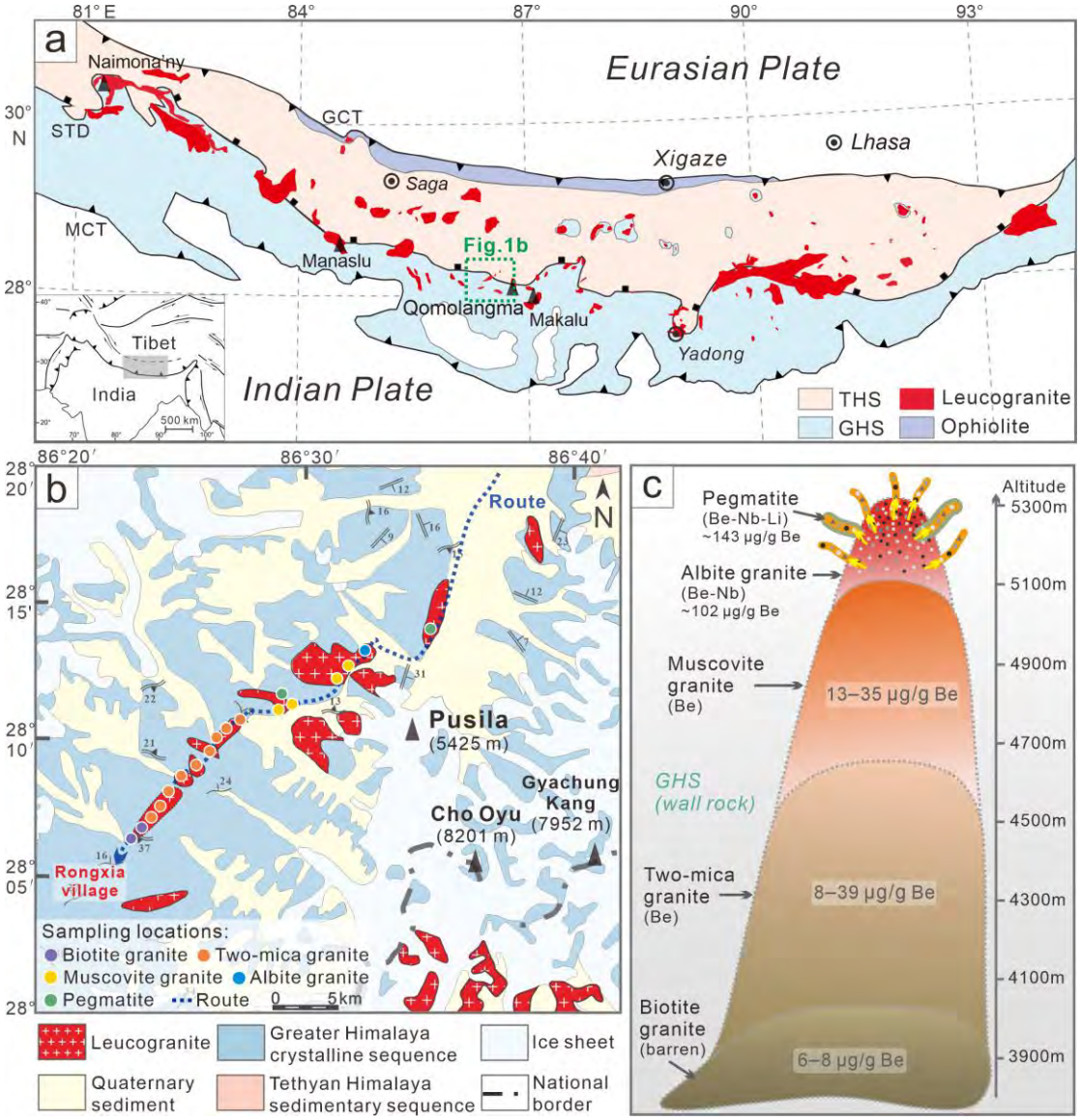

This is the peer-reviewed, final accepted version for American Mineralogist, published by the Mineralogical Society of America.
The published version is subject to change. Cite as Authors (Year) Title. American Mineralogist, in press.
DOI: https://doi.org/10.2138/am-2022-8353. http://www.minsocam.org/

Figure 2.

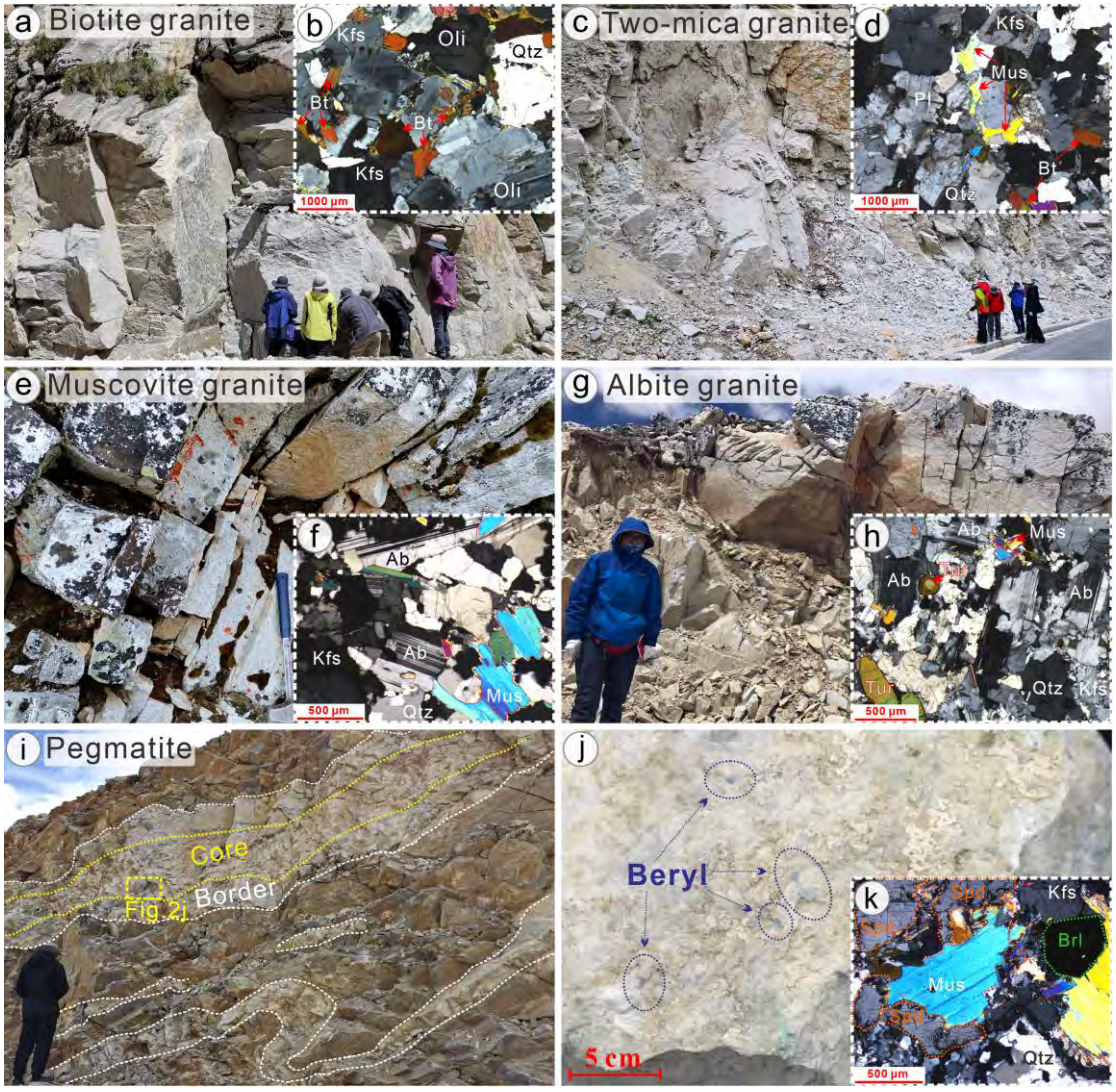

Figure 3.

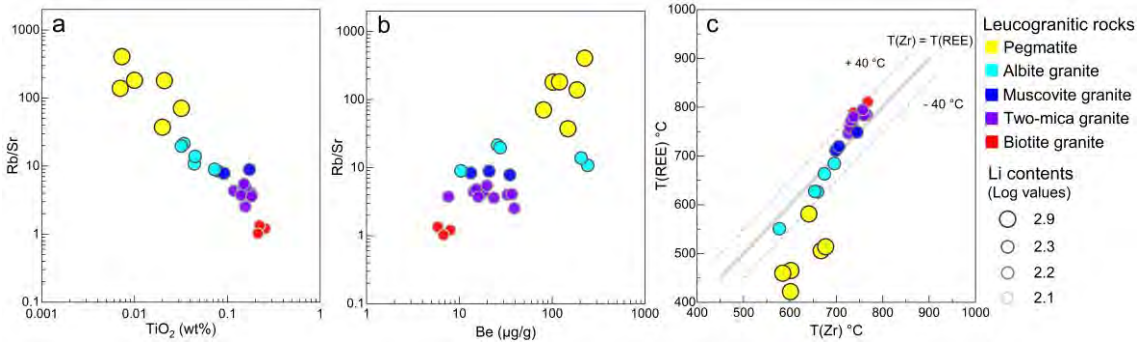

Figure 4.

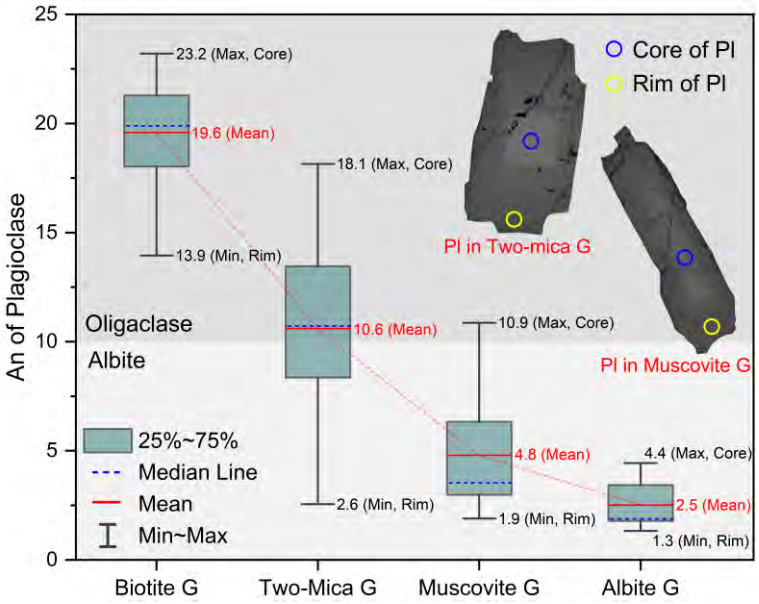

Figure 5.

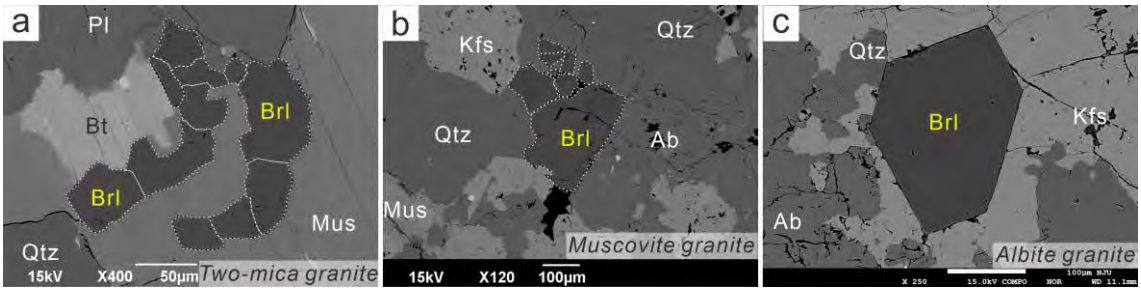

16 **Figure 6.**

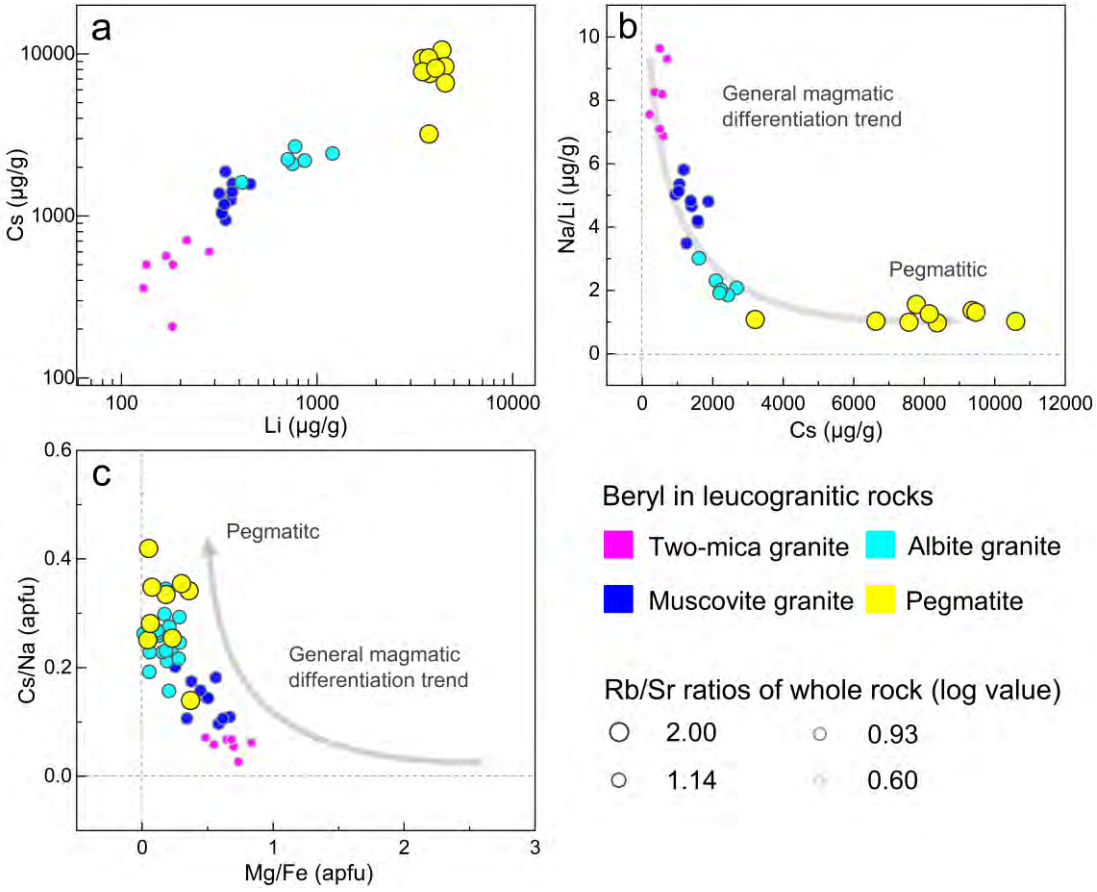

17

18

Figure 7.

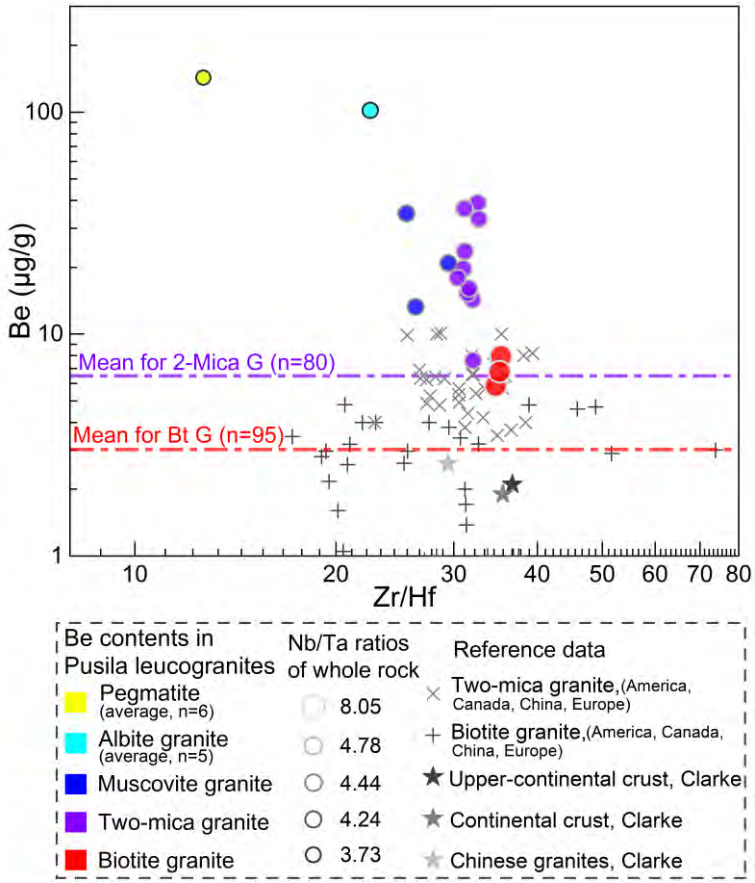

Figure 8.

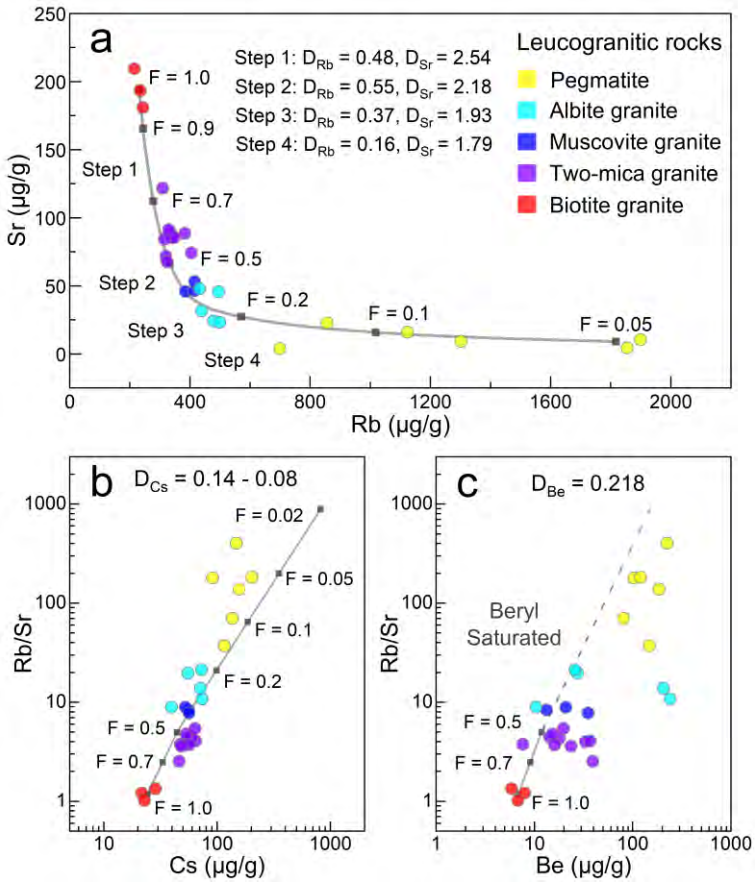

Figure 9.

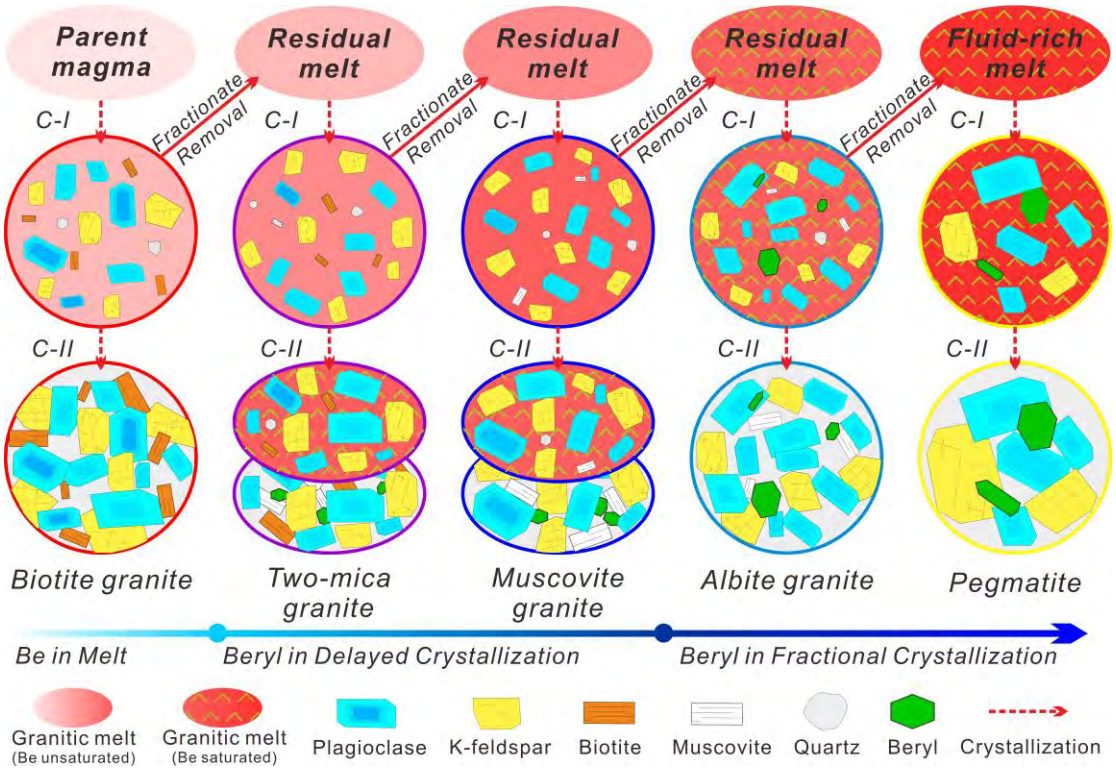

Table 1. Beryllium reservoirs in Pusila leucogranites.

	Biotite granite		Two-mica granite		Muscovite granite		Albite granite	
Temperature (°C)	774		756		721		641	
Be content of melt (ppm)	6–8	7^{ave}	8–39	22^{ave}	13–35	23^{ave}	10–241	102^{ave}
Mineral and Mode	fraction	Be	fraction	Be	fraction	Be	fraction	Be
K-feldspar	25%	0.9	28%	1.2	20%	1.3	10%	1.8
Plagioclase	42%	10.3	25%	9.2	30%	9.4	42%	11.2
Quartz	20%	0.8	30%	1.0	35%	0.0	40%	0.4
Muscovite	2%	10.0	8%	10.8	10%	11.3	3%	22.3
Biotite	10%	5.7	8%	5.2				
Tourmaline	1%	2.5	1%	4.4	4%	3.4	5%	5.4
Total Be in RFM (ppm):		6		4		4		6
Be in beryl (ppm)				18		19		96
Be in beryl (% total Be)				81%		81%		94%
Beryl in rock (Modal %)				0.04%		0.04%		0.19%

Abbreviation: RFM = rock-forming minerals; ^{ave}: average.

Table 2. Beryllium contents in biotite granites and two-mica granites worldwide.

Rock	Informations (country, location)	Number of samples	Mean Be content (ppm)	Data Source
Biotite granite	China, Canada, Czech, Karelia, Russia, Spain, Tuva, USA, Ukraine	95	***3***	1-10
Two-mica granite	China, Canada, Czech, Russia, Spain	80	***7***	1, 2, 4, 11-15
Other biotite and two-mica granites	China, Russia, Kazakhstan	48	***6***	2
All biotite and two-mica granites		223	***5***	

Data source: 1 = Bea et al., 1994; 2 = Beus, 1966; 3 = Breaks and Moore, 1992; 4 = Breiter et al., 1991; 5 = Chen et al., 2018; 6 = Lowell and Young, 1999; 7 = Tang, unpublished data; 8 = Tian et al., 2020; 9 = Xiang et al., 2020; 10 = Zhang et al., 2016; 11 = Breaks and Tindle, 2001; 12 = Chen et al., 2016; 13 = Ramírez and Grundvig, 1999; 14 = Ramírez and Grundvig, 2000; 15 = Zaraisky et al., 2009; see details in Supplemental Data 3.1.

Table 3. Beryllium contents in gneisses and pelitic rocks worldwide.

Rock	Other information	Location	Number of samples	Mean Be content (ppm)	Data Source
Gneiss	Himalaya, GHS	Pusila	3	***6***	1
Gneiss	Himalaya, GHS	Dinggye	8	*5*	2
Gneiss	Himalaya, GHS	Nyalam	5	*4*	3
Gneiss, Melanosomes			8	*5*	
Pelite	Himalaya, THS	Yala-Xiangbo	6	*5*	4
Pelitic rocks	unmetamorphosed	Worldwide	205	*3*	5
	metamorphosed	Worldwide	382	*3*	5

Data source: 1 = this study, Supplemental Data 3.2; 2 = Zhang et al., 2020; 3 = Yang, 2020; 4 = Aikman et al., 2012; 5 = Supplemental Data 3.3.

Table 4. Modeled Be content after partial melting.

Rock	MBS (22MS + 7Pl + 8Q → 25Melt + 5Kfs + 5Sil + 2Bt)[a]					
Mineral	$D_{mineral/melt}$ for Be	Origin	Consume	Produce	Restite	Recalculate
K-feldspar	0.19[b]	0%		7%	7%	9%
Plagioclase	1.84[b]	11%	8%		3%	4%
Quartz[c]	0.01	38%	10%		28%	40%
Muscovite	1.35[b]	29%	29%		0%	0%
Biotite	0.54[b]	13%		3%	16%	22%
Sillimanite[c]	0.01	4%		7%	11%	15%
Garnet[c]	0.01	6%			6%	9%
Modeled	Protolith	D_0	P	F	***Batch melting***	***Fractional melting***
Be	5.5 ppm	0.669	0.540	30%	***6.8 ppm***	***7.3 ppm***

The stoichiometry of muscovite dehydration-melting reaction from data: a = Patiño Douce and Harris, 1998; Be partition coefficients used for partial melting modelling from data: b = Evensen and London, 2002; c = Assumed.

Table 5. Rb-Sr-Be-Cs partition coefficients of main minerals for modeling Rayleigh fractionation.

Rock	Biotite granite					Two-mica granite					Muscovite granite					Albite granite				
	Fraction	D_{Rb}	D_{Sr}	D_{Be}	D_{Cs}	Fraction	D_{Rb}	D_{Sr}	D_{Be}	D_{Cs}	Fraction	D_{Rb}	D_{Sr}	D_{Be}	D_{Cs}	Fraction	D_{Rb}	D_{Sr}	D_{Be}	D_{Cs}
K-feldspar	25%	0.88[d]	5.00[b]	0.14[f]	0.13[d]	28%	0.89[d]	5.00[b]	0.14[f]	0.13[d]	20%	0.95[d]	5.00[b]	0.14[f]	0.13[d]	10%	0.95[d]	5.00[b]	0.14[f]	0.13[d]
Plagioclase	42%	0.05[d]	3.06[e]	0.37[f]	0.13[d]	25%	0.05[d]	3.06[e]	0.37[f]	0.13[d]	30%	0.04[d]	3.06[e]	0.37[f]	0.13[d]	42%	0.04[d]	3.06[e]	0.37[f]	0.13[d]
Quartz[a]	20%	0.01	0.01	0.01	0.01	30%	0.01	0.01	0.01	0.01	35%	0.01	0.01	0.01	0.01	40%	0.01	0.01	0.01	0.01
Muscovite	2%	1.60[c]	0.05[c]	0.87[f]	0.30[c]	8%	1.60[c]	0.05[c]	0.87[f]	0.30[c]	10%	1.60[c]	0.05[c]	0.87[f]	0.30[c]	3%	1.60[c]	0.05[c]	0.87[f]	0.30[c]
Biotite	10%	2.00[c]	0.04[c]	0.08[f]	0.40[c]	8%	2.00[c]	0.04[c]	0.08[f]	0.40[c]										
Total		***0.48***	***2.54***	***0.22***	***0.14***		***0.55***	***2.18***	***0.21***	***0.13***		***0.37***	***1.93***	***0.23***	***0.10***		***0.16***	***1.79***	***0.20***	***0.08***

Data sources: a = Assumed for quartz; b = Long, 1978; c = Icenhower and London, 1995; d = Icenhower and London, 1996; e = Drake and Weill, 1975; f = Evensen and London, 2002.

This is the peer-reviewed, final accepted version for American Mineralogist, published by the Mineralogical Society of America.
The published version is subject to change. Cite as Authors (Year) Title. American Mineralogist, in press.
DOI: https://doi.org/10.2138/am-2022-8353. http://www.minsocam.org/

Table 6. Beryllium partition coefficients of beryl.

Experiment[a]	HGS5+Brl+Qtz, R^2=0.9431, 200 MPa		
Temperature (°C)	640	720	750
Beryl solubility in melt (ppm)[a]	121	305	406
Be content in beryl ($Be_3Al_2(SiO_3)_6$, ppm)	50300	50300	50300
Be partition coefficients of beryl			
Be (in beryl, ppm) / Be (in melt, ppm)	416	165	124

Data sources: a = Evensen et al., 1999.

Table 7. Beryllium partition coefficients of whole rock (including beryl).

Rock	Biotite granite	Two-mica granite	Muscovite granite	Albite granite
Temperature (°C)	774	756	721	641
Be content of rock (ppm)	7 (6–8)	22 (8–39)	23 (13–35)	102 (10–241)
Mineral and Modal (%)				
Beryl[a]		0.04%	0.04%	0.19%
Be partition coefficient				
Rock-forming minerals[b]	0.22	0.21	0.23	0.20
Beryl[c]		416	165	124
Whole rock (including Beryl)	0.22	0.26	0.29	0.99

Data sources: a = Table 1; b = Table 5; c = Table 6.